NJC

ROYAL SOCIETY OF CHEMISTRY

PAPER

View Article Online
View Journal

CrossMark
click for updates

Cite this: DOI: 10.1039/c5nj03159a

# Zn(II) and Cu(II) formamidine complexes: structural, kinetics and polymer tacticity studies in the ring-opening polymerization of ε-caprolactone and lactides†

Ekemini D. Akpan,[a] Stephen O. Ojwach,*[b] Bernard Omondi*[a] and
Vincent O. Nyamori[a]

Treatment of *N*,*N*′-bis(2,6-dimethylphenyl)formamidine (**L1**), *N*,*N*′-bis(2,6-diisopropylphenyl)formamidine (**L2**), and *N*,*N*′-dimesitylformamidine (**L3**) with $Zn(OAc)_2{\cdot}2H_2O$ or $Cu(OAc)_2{\cdot}H_2O$ produced the corresponding Zn(II) and Cu(II) *N*,*N*′-diarylformamidine complexes $[Zn_3(\mathbf{L1})_2(OAc)_6]$ (**1**), $[Zn_2(\mathbf{L2})_2(OAc)_4]$ (**2**), $[Zn_2(\mathbf{L3})_2(OAc)_4]$ (**3**) and $[Cu_2(\mathbf{L2})_2(OAc)_4]$ (**4**), respectively. While complex **1** is trinuclear, compounds **2–4** are dimeric in the solid state. The X-band EPR spectra of complex **4** in solid and solution states are consistent with perfect axial symmetry and confirm retention of the dinuclear paddle-wheel core in the solution state. Complexes **1–4** formed active catalysts in the ring opening polymerization (ROP) of ε-caprolactone (ε-CL) and lactides (LA). Complexes **1** and **3** exhibited higher rate constants of 0.1009 $h^{-1}$ and 0.0963 $h^{-1}$ compared to the rate constants of 0.0479 $h^{-1}$ and 0.0477 $h^{-1}$ observed for **2** and **4**, respectively, in the ROP of ε-CL at 110 °C. Higher rate constants of 0.5963 $h^{-1}$ and 1.2962 $h^{-1}$ were obtained for complexes **1** and **3** in the ROP of LAs compared to those reported in the ROP of ε-CL at 110 °C. Activation parameters were determined as $\Delta H^{\ddagger} = 25.08\ \mathrm{kJ\ mol^{-1}}$ and $\Delta S^{\ddagger} = -201.7\ \mathrm{J\ K^{-1}\ mol^{-1}}$ for the ROP of ε-CL using **3**. Investigation of the kinetics of polymerization of ε-CL and LAs revealed first order dependence of the polymerization reactions on monomer concentration. Moderate molecular weight polymers of up to 21 286 g $mol^{-1}$ exhibiting relatively moderate molecular weight distributions and moderately heterotactic PLAs with Pr up to 0.65 were obtained.

Received (in Victoria, Australia)
9th November 2015,
Accepted 10th February 2016

DOI: 10.1039/c5nj03159a

www.rsc.org/njc

## Introduction

Polyesters obtained from renewable resources are fast replacing petrochemical-based plastics due to their biocompatible and biodegradable nature. As a result polyesters have found applications in the fields of agriculture,[1] packaging,[2] biomedical,[3] and pharmaceutical industries.[4] Ring-opening polymerization (ROP) has remained the most effective method for the synthesis of polycaprolactone (PCL) and polylactides (PLA) giving polymers with high molecular weights, low polydispersity indices (PDI) and specific stereo-microstructures for PLA.[5–7] The development of new catalysts or initiators for ROP of esters has generated great interest. Zn(II) and Cu(II) complexes have been shown to produce effective catalysts for the ROP reactions of cyclic esters largely because they are easily synthesized, stable, less toxic and more importantly biocompatible.[8]

The catalytic activities of β-diketiminate complexes employed in the ROP reactions of cyclic esters have been studied extensively.[9–11] Reports on amidine and amidinate complexes employed for ROP catalysis of cyclic esters are extremely rare.[12] Amidinate ligands have found many applications in coordination chemistry and also as ancillary ligands to form complexes as catalysts/initiators in organic transformation and polymerization reactions.[13,14] The flexibility of amidine and amidinate ligands to coordinate either as monodentate or as chelating ($\eta^2$) ligands renders their respective complexes very promising for application in catalysis.[15] The steric bulk of the ligand affects the coordination mode around the metal centers, and largely influences the control of polymer microstructure, and as such, careful design of the ligand motif

---

[a] *School of Chemistry and Physics, Westville Campus, University of KwaZulu-Natal, Private Bag X54001, Durban, 4000, South Africa. E-mail: owaga@ukzn.ac.za*
[b] *School of Chemistry and Physics, Pietermaritzburg Campus, University of KwaZulu-Natal, Private Bag X01, Scottsville, 3209, South Africa. E-mail: ojwach@ukzn.ac.za*

† Electronic supplementary information (ESI) available: The supplementary figures and Tables S1–S19 represent NMR spectra of complexes **1–3**, COSY and NOESY NMR spectra of complex **1**, DOSY NMR spectra of complexes **1** and **3**, graphs of percentage conversions of ε-CL to PCL, lactides to PLAs, plots of $\ln[\mathrm{CL}]_0/[\mathrm{CL}]_t$ *vs.* time at different concentrations and temperatures, GPC chromatograms, ESI-MS spectra of LA, and homonuclear decoupled $^1H$ NMR and $^{13}C$ NMR of PLAs, respectively, as discussed in this study. CCDC 1413137 (**1**), 1413165 (**2**), 1413216 (**3**) and 1413168 (**4**). For ESI and crystallographic data in CIF or other electronic format see DOI: 10.1039/c5nj03159a

could result in controlled ROP of cyclic esters.[16,17] The nature and chemical activities of the polymers obtained could be controlled *via* modification of the electronic and steric properties of amidine/amidinate ligands. Neutral mono (amidinate) and bi-functional ligands with two amidinate moieties bridged by a linker with rare earth metal complexes show catalytic activity towards cyclic ester polymerization, giving high molecular weight and narrow molecular weight distribution polymers.[18–20] Phomphrai and coworkers[21] reported rapid polymerization of ε-caprolactone and also found that bis(amidinate) tin(II) complexes with electron donating groups accelerated the polymerization reactions and enhanced the catalytic activities of the complexes.

In this paper, we report the synthesis of Zn(II) and Cu(II) formamidine complexes and their application as catalysts in the ROP of ε-CL and LAs. The expected structural rigidity offered by these formamidine ligands as opposed to the more flexible (pyrazolylmethy)pyridine synthons previously used may result in better control of the ROP reactions. A detailed structural study of the complexes and evaluation of the kinetics and polymer tacticity of these ROP reactions have been performed and are herein discussed.

## Experimental section

### General procedures

All experiments were carried out under argon using Schlenk techniques. All solvents were obtained from Sigma-Aldrich. Reagent grade ethanol was distilled and dried from magnesium turnings; dichloromethane (DCM) and hexane were dried from a sodium–benzophenone mixture. Metal salts ($Cu(OAc)_2{\cdot}H_2O$, $Zn(OAc)_2{\cdot}2H_2O$), and the monomers (ε-caprolactone and lactides) were obtained from Sigma-Aldrich. $^1H$ and $^{13}C$ NMR spectra were measured at room temperature using a Bruker 400 MHz spectrometer. $^1H$ NMR data were recorded in $CDCl_3$ listed as residual internal $CDCl_3$ ($\delta$ 7.26). Similarly, $^{13}C$ NMR data were recorded in $CDCl_3$ listed as residual internal $CDCl_3$ ($\delta$ 77.00). IR spectra were obtained on a PerkinElmer Universal ATR spectrum 100 FTIR spectrometer. Mass spectra of compounds were obtained from a Water synapt GR electrospray positive spectrometer.

### General procedure for ligand syntheses

Acetic acid (1.5 mole equivalents) was added to a round bottom flask charged with aniline (2 mole equivalents) and triethyl orthoformate (1 mole equivalent). The reaction mixture was heated under reflux and the temperature was maintained at 130–140 °C. After 3 h, the temperature was increased to 150 °C and all volatiles were removed *via* distillation. Upon cooling to room temperature, the reaction mixture solidified. The crude product was triturated with cold hexane and collected by vacuum filtration. The solid obtained was recrystallized in minimal hot acetone and stored at 4 °C. Crystals formed were collected *via* filtration and dried *in vacuo*, yielding the pure products (Scheme 1).

### Synthesis of Zn(II) and Cu(II) formamidine complexes

**$[Zn_3(L1)_2(OAc)_6]$ (1).** To a solution of $Zn(OAc)_2{\cdot}H_20$ (0.087 g, 0.396 mmol) in ethanol a solution of **L1** (0.200 g, 0.79 mmol) in ethanol was added dropwise. The resulting solution was stirred at room temperature for 24 h. The solvent was removed under vacuum, and the crude product was washed with hexane and recrystallized from the DCM/hexane solvent mixture to afford complex **1** as a white solid (0.281 g, 67.2%). $^1H$ NMR ($CDCl_3$, 400 MHz): $\delta$ (ppm) 1.99 (s, 18H, Ac $CH_3$), 2.32 (s, 24H, $CH_3$), 6.07–6.04 (d, $^3J$ = 10.9 Hz, 1H, NH), 7.22–7.04 (m, 12H, Ar), 7.74–7.71 (d, $^3J$ = 9.8 Hz, 1H, N=CH). $^{13}C$ NMR ($CDCl_3$, 400 MHz) $\delta$ (ppm) 180.2, 133.7, 129.0, 129.0, 128.5, 127.6, 22.9, 18.4, 17.7. IR (Nujol): $\nu$ = 3333 (w), 1630 (s), 1588 (s), 1471 (m). ESI-TOF MS: *m*/*z* (%); 391.28 $[LZn_2 + Li]^+$ (90), 569.26 $[L_2Zn + H]^+$ (35). Anal. calcd for $C_{46}H_{58}N_4O_{12}Zn_3$: C, 52.16; H, 5.90; N, 5.29. Found: C, 52.20; H, 6.10; N, 5.24.

**$[Zn_2(L2)_2(OAc)_4]$ (2).** The reaction of compound **L2** (0.150 g, 0.410 mmol) and $Zn(OAc)_2{\cdot}H_20$ (0.045 g, 0.021 mmol) in ethanol afforded complex **2** as a crystalline white solid (0.150 g, 68%). $^1H$ NMR ($CDCl_3$, 400 MHz): $\delta$ (ppm) $\delta$ (ppm) 1.18–1.19 (d, $^3J$ = 6.80 Hz, 48H, $CH_3$), 1.89 (s, Ac $CH_3$, 6H), 3.33–3.30 (m, 8H, CH), 7.24–7.11 (m, 12H, Ar), 7.38–7.35 (d, $^3J$ = 11.7 Hz, 1H, N=CH), 5.72–5.70 (d, $^3J$ = 11.8 Hz, 1H, NH). IR (Nujol): $\nu$ = 2960 (m), 1661 (s), 1587 (m), 1382 (w). ESI-TOF MS: *m*/*z* (%); 731.58 $[LZn_2(OAc)_4 - H]^+$ (45); 792 $[L_2Zn]^+$ (100). Anal. calcd for $C_{58}H_{84}N_4O_8Zn_2$: C, 63.55; H, 7.72; N, 5.11. Found: C, 63.30; H, 7.66; N, 5.12.

**$[Zn_2(L3)_2(OAc)_4]$ (3).** The reaction of compound **L3** (0.130 g, 0.464 mmol) and $Zn(OAc)_2{\cdot}H_20$ (0.050 g, 0.023 mmol) in ethanol afforded the crude product. The crude product was washed with hexane and recrystallized from the DCM/hexane solvent mixture to afford complex **3** as a white solid (0.176 g, 82%). $^1H$ NMR ($CDCl_3$, 400 MHz): $\delta$ (ppm) 1.97 (s, 12H, Ac $CH_3$), 2.27–2.18 (m, 36H, $CH_3$), 5.99–5.96 (d, $^3J$ = 11.9 Hz, 1H, NH), 6.93–6.84 (m, 8H, Ar), 7.67–7.65 (d, $^3J$ = 9.5 Hz, 1H, N=CH). $^{13}C$ NMR ($CDCl_3$, 400 MHz) $\delta$ (ppm) 137.3, 133.7, 129.0, 129.0, 22.9, 20.8, 18.4, 18.3, 17.6. IR (Nujol): $\nu$ = 3147 (w), 2915 (m), 1641 (s), 1556 (m),

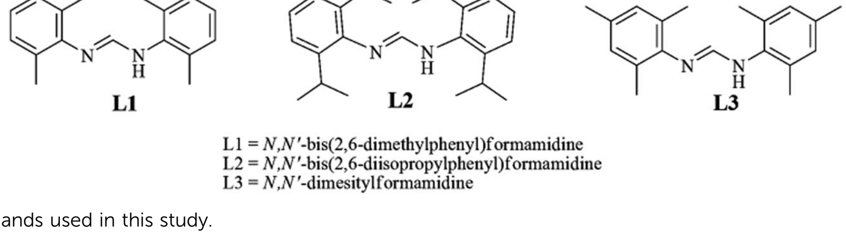

Scheme 1 Formamidine ligands used in this study.

1478 (s), 1432 (s), 1369 (m). ESI-TOF MS: *m*/*z* (%); 561 $[LZn_2(OAc)_2 + K]^+$ (100), 812.28 $[L_2Zn_2(OAc)_2 + Na]^+$ (20). Anal. calcd for $C_{46}H_{60}N_4O_8Zn_2$: C, 59.42; H, 6.72; N, 6.03. Found: C, 59.07; H, 6.52; N, 6.19.

**$[Cu_2(L2)_2(OAc)_4]$ (4).** The reaction of compound **L2** (0.200 g, 0.55 mmol) and $Cu(OAc)_2{\cdot}2H_20$ (0.050 g, 0.250 mmol) in ethanol afforded the crude product. The crude product was washed with hexane and recrystallized from the DCM/hexane solvent mixture to afford complex **4** as a light green solid (0.200 g, 74%). IR (Nujol): $\nu$ = 3264 (w), 2963 (m), 2866 (w), 1652 (s), 1621 (s), 1436 (s), 1412 (s). ESI-TOF MS: *m*/*z* (%); 791.50 $[M^+ - 4OAc]$ (100). Anal. calcd for $C_{58}H_{84}N_4O_8Cu_2$: C, 63.54; H, 8.09; N, 5.11. Found: C, 63.20; H, 7.79; N, 5.19.

### General procedure for bulk polymerization of ε-caprolactone

Bulk polymerization reactions were performed by introducing an appropriate amount of the complex and the ε-CL monomer (1.14 g, 0.01 mol) was added to a Schlenk tube immersed in a pre-heated oil bath at 110 °C and the reaction was initiated by stirring. Kinetics experiments were carried out by withdrawing samples at regular intervals using a syringe and quenching quickly by rapid cooling into an NMR tube containing $CDCl_3$ solvent using ice water. The quenched samples were analyzed by $^1$H NMR spectroscopy for the determination of polymerization of ε-CL to PCL. The percentage conversion of $[PCL]/[CL]_0 \times 100$, where $[CL]_0$ is the initial concentration of the monomer and [PCL] is the concentration of the polymer at time *t*, was evaluated by integration of the peaks for CL (4.2 ppm, $OCH_2$ signal) and PCL (4.0 ppm, $OCH_2$ signal) according to the equation $[PCL]/[CL]_0 = I_{4.0}/(I_{4.2} + I_{4.0})$, where $I_{4.2}$ is the intensity of the CL monomer signal at 4.2 ppm and $I_{4.0}$ is the intensity of the PCL signal at 4.0 ppm for $OCH_2$ protons. The observed rate constants were extracted from the slope of the line of best fit of the plot of $\ln[CL]_0/[CL]_t$ *vs.* time.

### Polymerization of D,L-LA and L-LA

A suitable lactide (1.44 g, 0.01 mol) was dissolved in toluene in a Schlenk tube equipped with a magnetic stirrer under argon and the required amount of the complex was added. The reaction mixture was stirred at 110 °C. Kinetics experiments were carried out by withdrawing samples at regular intervals using a syringe and quenching quickly by rapid cooling into an NMR tube containing $CDCl_3$ solvent using ice water. The quenched samples were analyzed by $^1$H NMR spectroscopy for the determination of polymerization of lactides to PLA. The integration values of the methine proton of the monomer and that of the polymer were used to calculate the percentage conversion using the equation $I_{\mathrm{CH\,monomer}}/(I_{\mathrm{CH\,monomer}} + I_{\mathrm{CH\,polymer}}) \times 100$.

### Polymer characterization by size exclusion chromatography (SEC)

The samples were analyzed by size exclusion chromatography at Stellenbosch University. The samples were dissolved in BHT stabilized THF (2 mg ml$^{-1}$). Sample solutions were filtered *via* a syringe through 0.45 μm nylon filters before being subjected to analysis. The SEC instrument consists of a Waters 1515 isocratic HPLC pump, a Waters 717plus auto-sampler, a Waters 600E system controller (run by Breeze Version 3.30 SPA) and a Waters in-line Degasser AF. A Waters 2414 differential refractometer was used at 30 °C in series along with a Waters 2487 dual wavelength absorbance UV/Vis detector operating at variable wavelengths. Tetrahydrofuran (THF, HPLC grade, stabilized with 0.125% BHT) was used as the eluent at flow rates of 1 ml min$^{-1}$. The column oven was kept at 30 °C and the injection volume was 100 μl. Two PLgel (Polymer Laboratories) 5 μm Mixed-C (300 × 7.5 mm) columns and a pre-column (PLgel 5 μm Guard, 50 × 7.5 mm) were used. Calibration was done using narrow polystyrene standards ranging from 580 to $2 \times 10^6$ g mol$^{-1}$. All molecular weights were reported as polystyrene equivalents.

### X-ray crystallography

The crystal evaluation and data collection of **1**, **2**, **3**, and **4** were done on a Bruker Smart APEXII diffractometer with Mo Kα radiation ($\lambda$ = 0.71073 Å) equipped with an Oxford Cryostream low temperature apparatus operating at 100 K for all samples. Reflections were collected at different starting angles and the APEXII program suite was used to index the reflections.[22] Data reduction was performed using the SAINT[23] software and the scaling and absorption corrections were applied using the SADABS[24] multi-scan technique. The structures were solved by the direct method using the SHELXS program and refined.[25] Graphics of the crystal structures were drawn using OLEX2 software.[26] Non-hydrogen atoms were first refined isotropically and then by anisotropic refinement with the full-matrix least squares method based on $F^2$ using SHELXL.[25] All hydrogen atoms were positioned geometrically, allowed to ride on their parent atoms and refined isotropically. Disorder was found for one of the isopropyl methyl groups of complex **2**. The electron density was observed in the difference map and used to model the disorder using PART instructions resulting in 58% occupancy of the major component. The C–C bond distance in the disordered methyl group was subjected to distance restraint, DFIX. Disorder was also found for one of the oxygen atoms of the acetate anions in complex **3** in which the electron density was observed in the difference map. The disorder was modelled using PART instructions resulting in an ~60% occupancy of the major component. Distant restraints (DFIX, DANG and SADI) were used to improve the C=O bond length in the disordered oxygen atoms of the acetate anions. Crystal data collection and structural refinement parameters for complexes **1–4** are provided in the ESI (Table S1, ESI†).

## Results and discussion

### Synthesis of *N*,*N*′-diarylformamidine Zn(II) and Cu(II) complexes

The *N*,*N*′-diarylformamidine ligands, *N*,*N*′-bis(2,6-dimethylphenyl)-formamidine (**L1**), *N*,*N*′-bis(2,6-diisopropylphenyl)formamidine (**L2**), and *N*,*N*′-dimesitylformamidine (**L3**), were synthesized following the literature procedure.[27,28] Reactions of **L1–L3** with two molar equivalents of $Zn(OAc)_2{\cdot}2H_2O$ or $Cu(OAc)_2{\cdot}H_2O$ salts afforded the corresponding trinuclear and dinuclear Zn(II) and Cu(II) complexes $[Zn_3(\mathbf{L1})_2(OAc)_6]$ (**1**), $[Zn_2(\mathbf{L2})_2(OAc)_4]$ (**2**),

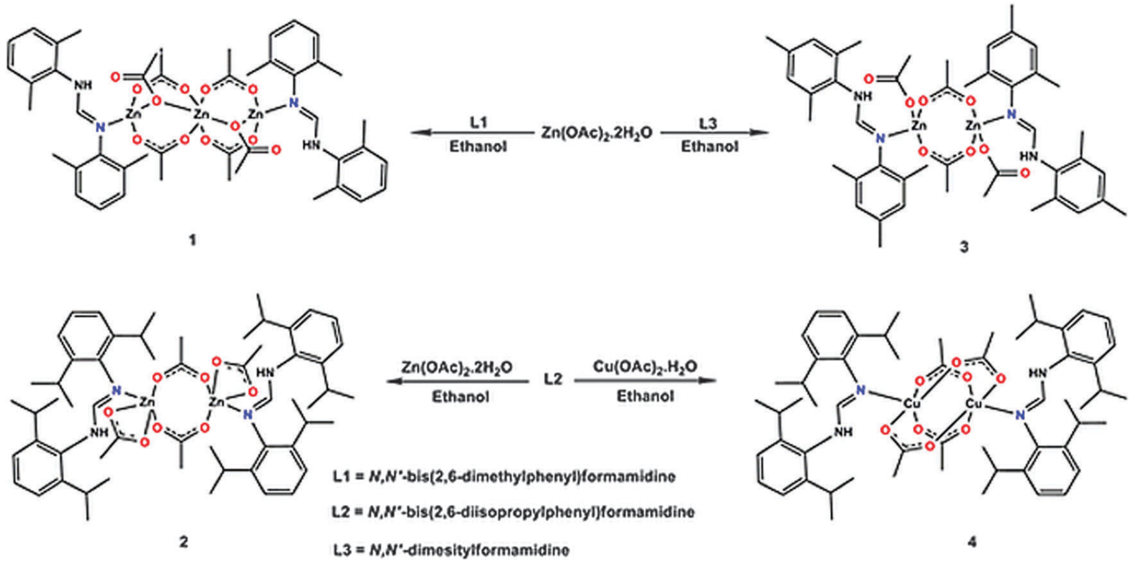

Scheme 2 Synthesis of Zn(II) and Cu(II) formamidine complexes **1–4**.

$[Zn_2(\mathbf{L3})_2(OAc)_4]$ (**3**) and $[Cu_2(\mathbf{L2})_2(OAc)_4]$ (**4**) in moderate to high yields (Scheme 2). Complexes **1–3** were isolated as white solids, while complex **4** was obtained as a green solid.

Complexes **1–3** were characterized using $^1H$ and $^{13}C$ NMR spectroscopy (Fig. S1 to S5, ESI†), mass spectrometry, IR spectroscopy, elemental analyses and single crystal X-ray crystallography. COSY spectra of complex **1** showed correlation between aromatic protons (7.16–7.04 ppm) and the $CH_3$ protons on the phenyl ring. A perfect correlation also existed between the NH proton (6.07–6.04 ppm) and the CH=N methine proton (7.74–7.71 ppm) (Fig. S6, ESI†). The cross peaks in the NOESY spectrum (Fig. S7, ESI†) could be due to cross relaxation between neighboring protons in the ligand motif.[29] A distance of 2.779 Å between the two types of protons was measured in the crystal structure of complex **1**, affirming the NOESY NMR spectra. Mass spectra of complexes **1–4** showed *m*/*z* peaks corresponding to various fragments of the parent compounds. For example, complex **3** showed a $m/z = 645.13$ corresponding to $[LZn_2(OAc)_4 + H]^+$. FTIR spectra of complexes **1–4** displayed the characteristic carbonyl bands assignable to the $\nu_{asym}$ (OCO) and $\nu_{sym}$ (OCO) of the acetate ligands, respectively.[30] For example, the IR spectrum of complex **1** revealed two bands at 1639 $cm^{-1}$ and 1588 $cm^{-1}$ assignable to $\nu_{asym}$ (OCO) while the bands at 1471 $cm^{-1}$, 1404 $cm^{-1}$, and 1373 $cm^{-1}$ could be attributed to $\nu_{sym}$ (OCO). The measured effective magnetic moment of the paramagnetic complex **4** at room temperature was 1.97 BM, signifying significant Cu···Cu interaction.[31]

### Molecular structures of complexes 1, 2, 3 and 4

X-ray quality crystals of complexes **1–4** were obtained by slow diffusion of hexane into dichloromethane solutions of the respective complexes. Fig. 1–4 show the molecular structures of complexes **1–4**, respectively, while selected bond distances and angles are under the captions of each figure. The asymmetric unit of the trinuclear complex **1** has half a molecule of the complex with the other half generated by a center of inversion at the central Zn atom. Dinuclear complex **2** has one full molecule and two half molecules in the asymmetric unit and the molecules in **2** are related by a d-glide. Dinuclear complex **3** has two half molecules in its asymmetric unit with the other halves generated by a center of inversion located at ⟨1 1 1⟩ in one half and at ⟨1/2 1/2 1/2⟩ in the other half. The two full molecules are related by an n-glide but are however having different acetate environments as discussed later in this section. Complex **4** has half a molecule in the asymmetric unit.

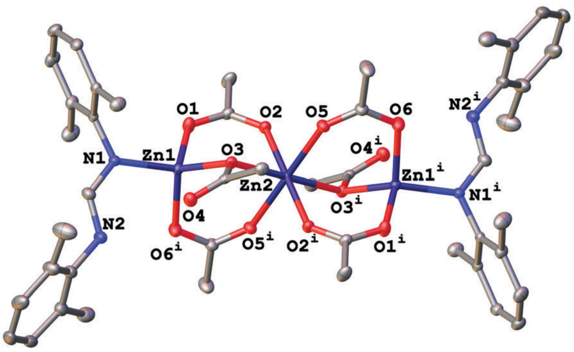

Fig. 1 X-ray crystal structure of complex **1** with thermal ellipsoids drawn at 40% probability level. Hydrogen atoms have been omitted for clarity. Selected bond lengths (Å) and angles (°): Zn(1)–Zn(2) 3.2099(3), N(1)–Zn(1) 1.9932(13), O(2)–Zn(2) 2.0312(11), O(1)–Zn(1) 1.9581(12), N(1)–C(9) 1.299(2), N(2)–C(9) 1.325(2), O(3)–Zn(2) 2.1441(10), Zn(1)–O(3)–Zn(2) 102.97(4), O(3)–Zn(1)–O(1) 104.24(5), O(2)–Zn(2)–O(3) 90.39(4), O(3)–Zn(1)–N(1) 123.34(5), O(1)–Zn(1)–N(1) 108.04(5), and $O(6)^i$–Zn(1)–N(1) 101.75(5). Symmetry transformations used to generate equivalent atoms: (i) = $-x + 1$, $-y + 1$, $-z + 1$.

The coordination to the metal centers in all four complexes is through the imine N atom of the formamidine ligands (in a monodentate fashion) and O atoms of acetate anions in the remaining coordination sites in monodentate, bidentate or bridging fashions. The three Zn(II) centers in complex **1** are

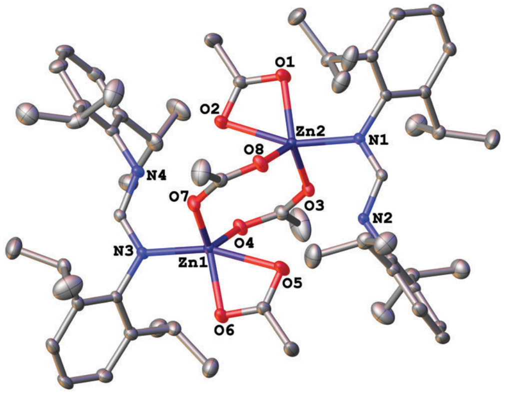

Fig. 2 X-ray crystal structure of complex **2** with thermal ellipsoids drawn at 40% probability level. Hydrogen atoms and the minor component of the disordered methyl groups have been omitted for clarity. Only one of the dimers in the asymmetry unit is shown for clarity. Selected bond lengths (Å) and angles (°): Zn(1)–Zn(2) 3.7648(6), N(1)–Zn(2) 2.0515(13), Zn(1)–O(6) 2.0256(12), Zn(2)–O(1) 2.0389(12), O(3)–Zn(2)–N(1) 97.05(5), O(1)–Zn(2)–O(3) 113.43(6), O(8)–Zn(2)–O(2) 91.50(5), N(1)–Zn(2)–O(1) 100.22(5).

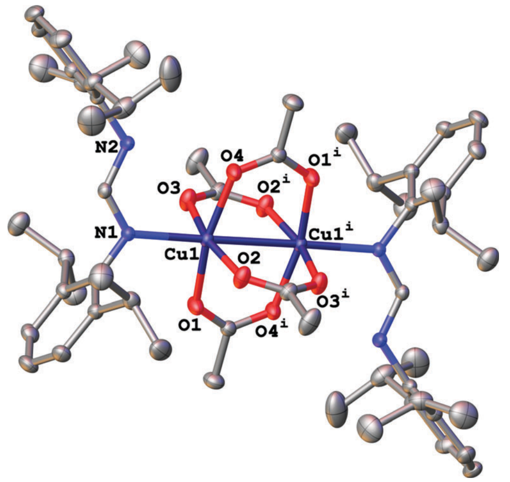

Fig. 4 X-ray crystal structure of complex **4** with thermal ellipsoids drawn at 30% probability level. Hydrogen atoms have been omitted for clarity. Selected bond lengths (Å) and angles (°): Cu(1)–Cu(1) 2.6797(5), N(1)–Cu(1) 2.1821(13), O(4)–Cu(1) 1.9891(13), O(3)–Cu(1) 1.9654(14), N(1)–Cu(1)–O(2) 100.55(5), O(1)–Cu(1)–O(4) 166.70(5), O(4)–Cu(1)–O(3) 87.21(6), symmetry code: (i) = $-x + 1$, $-y + 1$, $-z$.

arranged in a linear fashion revealing the two bridging modes. In total six acetate anions are involved in the bridging environment where four are in the bidentate while two are in the monodentate bridging mode. The acetate anions in the dinuclear complex **2** coordinate to the Zn(II) centers in two modes. Two are bridging in a bidentate mode resulting in an eight member bi-metallacycle with two Zn atoms and two O–C–O moieties of the acetate anion. Each of the remaining two are chelating to the Zn(II) centers in a bidentate manner based on bond distances and angles.[32] Complex **3** as mentioned earlier has two half molecules with the other halves generated by inversion. Both molecules form a similar eight member bi-metallacycle through two of the four acetate anions as in complex **2**. However the remaining two anions coordinate differently to the Zn(II) centers, one in an anisodentate fashion (Fig. 3a) and the other in a monodentate fashion (Fig. 3b). The conformations of the bi-metallacycle moieties in **3** are different from that of complex **2** and so is the coordination of the acetate anions probably due to steric influences. Complex **4** exhibits a familiar dinuclear paddle wheel conformation in which all four acetate anions bridge the two Cu(II) centers in a bidentate bridging mode.

The three Zn(II) centers in complex **1** adopt two coordination geometries in which the two axial Zn atoms are in a distorted tetrahedral environment with a N atom and three O atoms from the formamidine and the acetate anions, respectively, while the middle Zn atom is in a distorted octahedral environment in

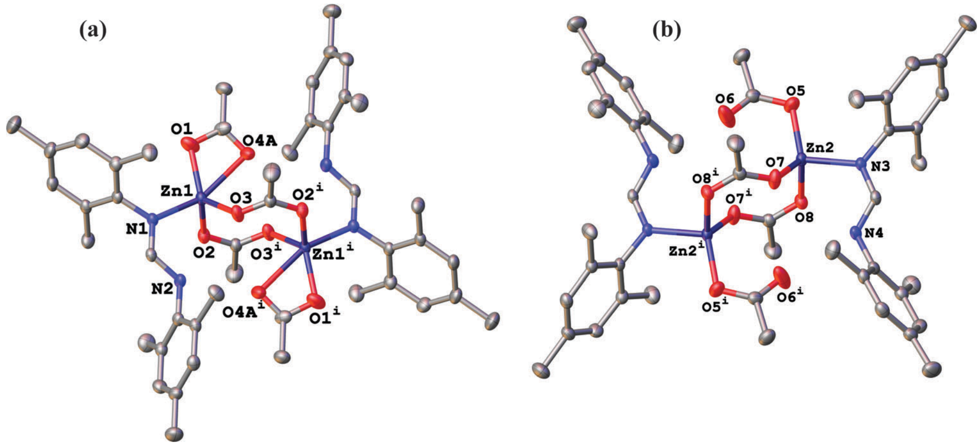

Fig. 3 X-ray crystal structure of complex **3** with thermal ellipsoids drawn at 30% probability level. Hydrogen atoms and the minor component of the disordered O atom have been omitted for clarity. Selected bond lengths (Å) and angles (°): (a) molecule with anisodentate coordination acetates, Zn(1)–N(1) 2.022(2), Zn(1)–O(2) 1.984(2), Zn(1)–O(1) 1.960(3), Zn(1)–O(4A) 2.34(2), O(1)–Zn(1)–O(2) 112.26(11), O(2)–Zn(1)–N(1) 98.58(9), O(3)–Zn(1)–O(2) 111.28(10), symmetry transformations used to generate equivalent atoms: (i) = $-x + 2$, $-y + 2$, $-z + 2$. (b) Molecule with monodentate coordination acetate, Zn(2)–N(3) 2.018(2), Zn(2)–O(5) 1.923(2), Zn(2)–O(7) 1.964(2), O(7)–Zn(2)–O(5) 121.90(11), O(7)–Zn(2)–N(3) 98.20(9), O(8)–Zn(2)–O(5) 111.61(11), symmetry transformations used to generate equivalent atoms: (ii) = 1 $-x + 1$, $-y + 1$, $-z + 1$.

which the equatorial and axial coordination site are occupied by O atoms. In complex **2** the geometries around the Zn atoms adopt a severely distorted trigonal bipyramidal geometry due to the coordination of one of the acetate anions being anisobidentate in manner, while the Zn(II) atoms in complex **3** adopt a distorted tetrahedral geometry in one of the molecules and a distorted trigonal pyramidal geometry in the second molecule. The distortions from a regular arrangement and the selective formation of either trinuclear and dinuclear complexes could be due to the flexibility in binding modes of the acetate ligands, in addition to steric restriction imposed by **L1–L3**, respectively.[17,33]

The trigonal planar nature of the secondary amine group suggests conjugation of the amine lone pair with the π-electron system of the aryl ring, possibly accounting for its apparently rather poor σ-donor strength, and could justify its inability to facilitate chelation of the metal ion.[34] The Zn–O bond distances in complexes **1–3** fall within the ranges of similar complexes in the literature.[35–42] Only one of these seems a little longer as seen in complex **2** and complex **3a**, respectively, resulting in anisobidentate chelating behavior.[20] The observed metal to metal distances in complexes **1–3** are greater than the sum of the van der Waals radii of Zn (1.39 Å) indicating the absence of any meaningful Zn–Zn interatomic metal bond *vis-à-vis* metal–metal interaction.[34] Complex **4** exhibit a Cu···Cu distance of 2.6796(3) Å typical of binuclear copper(II) acetates that possess N-donating apical ligands.[43]

In the crystals of all four complexes fairly strong intramolecular hydrogen bonds and interactions exist in which the acetate oxygen atoms are the acceptor atoms and the ligand N atoms the donor atoms. These interactions seem to play a significant role in the packing of the molecules in crystals.[37,40]

## Electron paramagnetic resonance spectra of complex 4

In order to understand the coordination environment of the paddle-wheel Cu(II) complex in both solid state and solution, X-band EPR spectra of complex **4** were acquired in methanol solution and in solid state at 295 K (Fig. 5). In methanol solution, the EPR spectrum of complex **4** (Fig. 5a) is almost perfectly isotropic and is characterized by a single line ($g = 2.1062$). This indicates that there is a total symmetric environment where the electrons in the different d-orbitals have equal interactions in all directions (all the principal $g$-factors are the same).

The spin-allowed $\Delta m_s = \pm 1$ transitions are thus degenerate and occur at a resonant frequency governed by $g^{iso}$. The significant $g$-shift of $g^{iso} = 2.1062$ to $g_e$ (2.0025) reflects the spin–orbit coupling effect in the paddle-wheel complex.[34] The solid state EPR spectrum (Fig. 5b) shows axial symmetry such that the total magnetic moment in the $Z$-direction is rather large ($g_x = g_y \neq g_z$). The magnetic parameters for the exchange-coupled copper–copper pairs are $g_{\parallel} = 2.3554$ and $g_{\perp} = 2.0840$. A consistent interpretation of these data is presented on the basis of a weak metal–metal interaction.[44] The similarity in the solution and solid state EPR spectra of complex **4** confirms the retention of the paddle-wheel structure in solution.

## Ring opening polymerization of ε-CL and LAs

The ROP reactions of ε-CL using complexes **1–4** as catalysts were initially investigated at 110 °C using the [M]/[catalyst] ratio of 200. Under these conditions, complexes **1–4** exhibited significant catalytic activities giving maximum conversions between 48 h and 76 h (Fig. S9a, ESI†). Complexes **1** and **3** were also investigated in the ROP of D,L-LA and L-LA at 110 °C using the [M]/[catalyst] ratio of 200 in toluene and afforded conversions of 97% and 99% within 3.5 and 9 h, respectively (Fig. S9b, ESI†). Tables 1 and 2 contain a summary of the ROP data of ε-CL and LAs for complexes **1–4**, respectively.

Having established that complexes **1–4** form effective catalysts in the ROP of ε-CL and LAs, we carried out detailed kinetic and polymer property studies to gain insight into the influence of catalyst structure and reaction conditions on the kinetics of the polymerization reactions and the nature of polymers obtained.

## Kinetics of ROP reactions of ε-CL and LAs

Kinetic studies of the ROP of ε-CL were investigated for complexes **1–4** and monitored by $^1$H NMR spectroscopy. The rates of the reaction were determined from the plot of $\ln[CL]_0/[CL]_t$ *versus* time

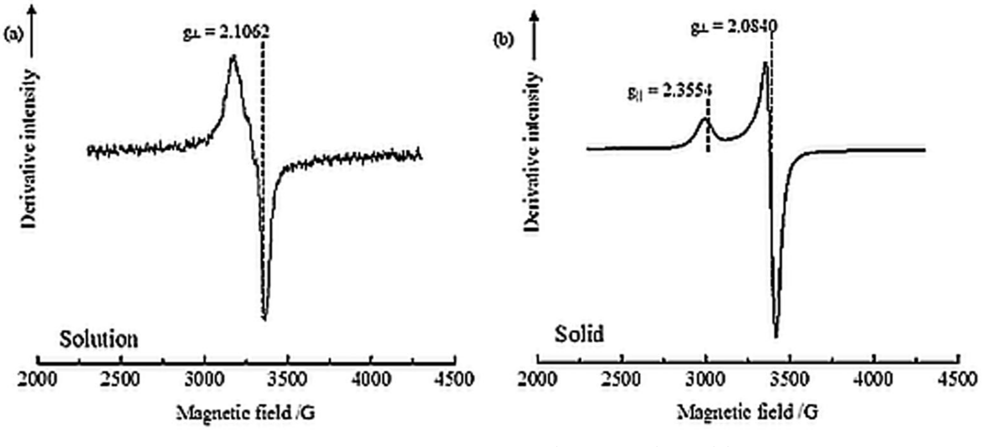

Fig. 5 (a) Room temperature EPR spectrum of complex **4** in methanol solution (9.786 GHz) and (b) solid state EPR spectrum of complex **4** (295 K, 9.870 GHz).

Table 1 Summary of polymerization data of ε-CL by complexes **1–4**[a]

| Catalyst | Time (h) | Conversion (%) | $k_{app}$ ($h^{-1}$) | $M_w$ (GPC)[b] | PDI[b] | IE[c] |
|---|---|---|---|---|---|---|
| 1 | 48 | 98 | 0.1009 | 12 632 | 2.11 | 0.56 |
| 2 | 72 | 96 | 0.0479 | 5426 | 1.86 | 0.25 |
| 3 | 53 | 96 | 0.0963 | 10 342 | 2.14 | 0.47 |
| 4 | 76 | 98 | 0.0441 | 3838 | 1.66 | 0.17 |

[a] Reaction conditions, bulk polymerization, 110 °C, $[CL]_0$/[catalyst] = 200. [b] Molecular-weight average and polydispersity index (PDI) determined by GPC relative to polystyrene standard values, the values obtained from GPC × correction factor of 0.56.[33] [c] Initiator efficiency (IE) = $M_{wexp}/M_{wcalc}$, where $M_{wcalc} = M_{w(monomer)} \times [CL]_0/[I] \times [PCL]/[CL]_0 + M_{w(chain\text{-}end\ group)}$.

Table 2 ROP of D,L-LA and L-LA using complexes **1** and **3**[a]

| Entry | Catalyst | Time (h) | Conversion[b] (%) | $k_{app}$ ($h^{-1}$) | $M_w$ (GPC)[c] | PDI[c] | IE[d] |
|---|---|---|---|---|---|---|---|
| 1[e] | **1** | 3.5 | 97 | 1.2765 | 10 376 | 2.25 | 0.37 |
| 2[f] | **1** | 5 | 96 | 0.8737 | 21 286 | 1.79 | 0.77 |
| 3[e] | **3** | 9 | 99 | 0.6412 | 15 867 | 1.99 | 0.55 |
| 4[f] | **3** | 9 | 99 | 0.5963 | 18 054 | 1.85 | 0.63 |

[a] Reaction conditions: $[CL]_0/[I]$ = 200; solvent, toluene; temperature, 110 °C. [b] Maximum conversion achieved. [c] Molecular-weight average and polydispersity index (PDI) determined by GPC relative to polystyrene standard values, the values obtained from GPC × correction factor of 0.58.[33] [d] Initiator efficiency (IE) = $M_{wexp}/M_{wcalc}$, where $M_{wcalc} = M_{w(monomer)} \times [CL]_0/[I] \times [PCL]/[CL]_0 + M_{w(chain\text{-}end\ group)}$. [e] D,L-LA. [f] L-LA.

(Fig. S10a, ESI†). Linear relationships consistent with *pseudo*-first-order dependency on the monomer were observed in all cases (Fig. S10a, ESI†). Thus, the rate of ε-CL polymerization can be written as shown in eqn (1):

$$\frac{d[CL]}{dt} = k[CL] \qquad (1)$$

where $k = k_p[I]^x$; $k_p$ is the rate of chain propagation, I is the initiator, and $x$ is the order of reaction.

The apparent rate constants for catalysts **1–4** in the ROP of ε-CL were extracted from Fig. S10a (ESI†) and are given in Table 1. More discerning was the drastic decrease in catalytic activity observed for catalyst **2** (0.0479 $h^{-1}$) bearing isopropyl groups relative to catalyst **1** (0.1009 $h^{-1}$) containing the less bulky methyl groups. Reduction of catalytic activity with an increase in the steric bulk of the ligand framework may be rationalized by inhibition of monomer coordination to the metal center.[45] Similar trends have been observed for bis(thiophosphinic amine) yttrium catalyst systems.[46]

Kinetic studies of the ROP of LAs were also investigated using complexes **1** and **3**. A linear relationship of the plot of $\ln[CL]_0/[CL]_t$ *versus* time was also obtained (Fig. S10b, ESI†) consistent with a *pseudo*-first-order dependency on LA concentration. The apparent rate constants for complexes **1** and **3** in the ROP of LAs were extracted from Fig. S10b (ESI†) and are given in Table 2. We observed that the reaction rates of ROP of ε-CL were much slower than those of LA reactions. This is in good agreement with literature findings and has largely been attributed to the larger ring size of ε-CL.[47] The six-membered ring in LA increases the strain resulting in rapid ROP reactions.[48]

## Order of ROP of ε-CL reaction with respect to catalysts 1 and 3

Polymerization reactions at different catalyst concentrations at constant ε-CL monomer concentration were carried out to determine the order of reaction with respect to catalysts **1** and **3** (Table 3). A plot of ln $k_{app}$ *versus* ln[**1**/**3**] gave linear relationships which allowed us to determine the order of reaction with respect to **1** and **3** (Fig. 6). The order of reaction with respect to **1** and **3** was extracted from the gradients of the lines of best fit (Fig. 6) and was obtained as 2.1420 ≈ 2 and 0.6343 respectively. Fractional orders of reaction with respect to catalysts have been previously reported and largely attributed to catalyst aggregation especially in bulk polymerization reactions.[15,49] The DOSY NMR experiment was carried out in order to ascertain if complexes **1** and **3** indeed undergo aggregation (Fig. S8, ESI†). The DOSY spectrum is consistent with the existence of one species in solution thereby negating the possibility of complex aggregation. A slight difference in the diffusion co-efficient of $1.666 \times 10^{-9}$ m$^2$ s$^{-1}$ and $1.112 \times 10^{-9}$ m$^2$ s$^{-1}$ was observed at 30 °C for **1** and **3**, respectively. More intriguing is the large difference in reaction orders with respect to catalysts **1** and **3**. This might be associated with the nuclearity and structures of the complexes; while complex **1** is trinuclear, complex **3** is dinuclear.

It is therefore conceivable to conclude that the active catalytic species produced from complexes **1** and **3** are structurally different and that the solid state structures are likely to be retained in solution. The overall order of the polymerization reactions catalyzed by complexes **1** and **3** could thus be described according to eqn (2) and (3) respectively:

$$\frac{d[CL]}{dt} = k[CL][\mathbf{1}]^2 \qquad (2)$$

$$\frac{d[CL]}{dt} = k[CL][\mathbf{3}]^{0.6} \qquad (3)$$

## Effect of solvent and temperature on the ROP kinetics of ε-CL

To understand the influence of solvent on the polymerization kinetics of ε-CL, we compared the activity of complex **3** in bulk and solution polymerization reactions. Table 4 shows a

Table 3 Effect of catalyst concentrations on the polymerization kinetics of ε-CL[a]

| Catalyst | $[CL]_0$/[Cat] | Time (h) | Conversion[b] (%) | $k_{app}$ ($h^{-1}$) | $M_w$ (GPC)[c] | PDI[c] | IE[d] |
|---|---|---|---|---|---|---|---|
| 1 | 100 | 18 | 97 | 0.2894 | 7666 | 2.01 | 0.69 |
| 1 | 150 | 30 | 97 | 0.1409 | 7879 | 2.36 | 0.47 |
| 1 | 250 | 48 | 96 | 0.0450 | 13 252 | 2.47 | 0.48 |
| 1 | 300 | 68 | 82 | 0.0252 | 13 646 | 2.15 | 0.49 |
| 3 | 100 | 30 | 97 | 0.1557 | 5141 | 1.91 | 0.46 |
| 3 | 150 | 48 | 98 | 0.1097 | 7864 | 2.41 | 0.47 |
| 3 | 250 | 48 | 95 | 0.0797 | 13 506 | 1.92 | 0.50 |
| 3 | 300 | 48 | 95 | 0.0781 | 14 124 | 2.14 | 0.43 |

[a] Reaction conditions, bulk polymerization, 110 °C. [b] Maximum conversion achieved. [c] Molecular-weight average and polydispersity index (PDI) determined by GPC relative to polystyrene standard values, the values obtained from GPC × 0.56.[33] [d] Initiator efficiency (IE) = $M_{wexp}/M_{wcalc}$, where $M_{wcalc} = M_{w(monomer)} \times [CL]_0/[Cat] \times [PCL]/[CL]_0 + M_{w(chain\text{-}end\ group)}$.

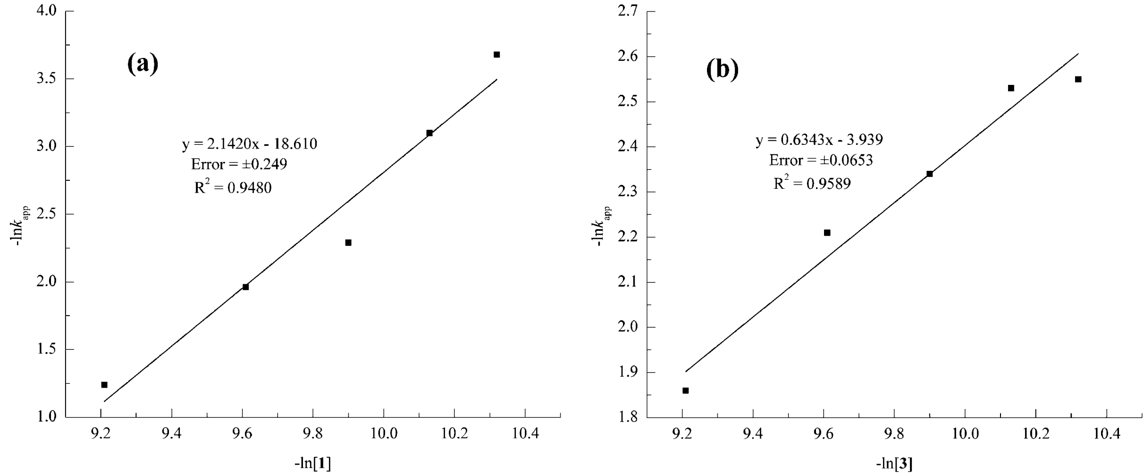

Fig. 6 (a) Plot of $\ln k_{app}$ *vs.* ln[**1**] and (b) $\ln k_{app}$ *vs.* ln[**3**] for the determination of order of reactions with respect to catalysts **1** and **3**.

summary of the bulk and solution ROP data of ε-CL and at different reaction temperatures. The rate of polymerization reactions recorded in toluene solvent was comparable to that in the bulk experiment (Table 3). This contrasts previous reports where we observed higher catalytic activities in bulk reactions in comparison to solution experiments.[16]

The dependence of the kinetics of the ROP of ε-CL reaction on reaction temperature was studied by determination of the rate constants at various temperatures (60 °C to 110 °C) using complex **3** (Fig. S11, ESI†). After induction periods observed at lower temperatures, linear relationships consistent with pseudo first-order dependency on the monomer were observed. A significant decrease in the rate constant from 0.0963 $h^{-1}$ to 0.064 $h^{-1}$ was recorded with the decrease in the reaction temperature from 110 °C to 90 °C. The observed rate constants extracted from the semi-logarithmic plots (Fig. S11, ESI†) are shown in Table 4.

The overall activation energy of the ROP of ε-CL using complex **3** calculated from the slope of the Arrhenius plot of $\ln k$ *vs.* $T^{-1}$ was found to be 28.05 kJ $mol^{-1}$ (Fig. 7a). This value is lower than that reported for ROP reactions using the lanthanide tris(2,4,6-tri-*tert*-butylphenolate) catalyst of 39.3 kJ $mol^{-1}$[50] but higher than the value of 12.05 kJ $mol^{-1}$ reported by Mei and co-workers.[49] The low energy barrier hints at a greater number of active sites in the system at lower temperatures. From the Eyring plot in Fig. 7b, the enthalpy of activation $\Delta H^{\ddagger}$ and the entropy of activation $\Delta S^{\ddagger}$ were obtained as 25.08 kJ $mol^{-1}$ and −201.7 J $K^{-1}$ $mol^{-1}$, respectively, for complex **3** at $[CL]_0/[I]$ = 200. These results are consistent with highly ordered transition state systems and are in good agreement with those reported for coordination-insertion mechanisms in the ROP of ε-CL.[51,52]

Table 4 Effect of solvents and reaction temperature on the polymerization kinetics of ε-CL using complex **3**

| Entry | $[CL]_0/[I]$ | Time (h) | Conversion[a] (%) | $k_{app}$ ($h^{-1}$) | $M_w$ (GPC)[b] | PDI[b] | IE[c] |
|---|---|---|---|---|---|---|---|
| 1 | 200[d] | 52 | 98 | 0.0778 | 7073 | 2.02 | 0.32 |
| 2 | 200[e] | 96 | 97 | 0.0640 | 4108 | 1.74 | 0.19 |
| 3 | 200[f] | 156 | 97 | 0.0371 | 2186 | 1.46 | 0.10 |
| 4 | 200[g] | 168 | 93 | 0.0283 | 4319 | 1.76 | 0.20 |
| 5 | 200[h] | 240 | 95 | 0.0257 | 2153 | 1.43 | 0.10 |

[a] Maximum conversion achieved. [b] Molecular-weight average and polydispersity index (PDI) determined by GPC relative to polystyrene standard values, the values obtained from GPC × 0.56.[33] [c] Initiator efficiency (IE) = $M_{wexp}/M_{wcalc}$, where $M_{wcalc} = M_{w(monomer)} \times [CL]_0/[I] \times [PCL]/[CL]_0 + M_{w(chain\text{-}end\ group)}$. [d] Solvent, toluene. [e] Temp., 90 °C. [f] Temp., 80 °C. [g] Temp., 70 °C. [h] Temp., 60 °C.

### Molecular weight and molecular weight distribution of polymers

The molecular weight and molecular weight distribution of polymers obtained were determined by GPC and compared with the theoretical values calculated from $^1H$ NMR spectra (Tables 1–4). Generally higher molecular weights of up to 21 286 g $mol^{-1}$ were obtained for PLA compared to the maximum value of 14 124 g $mol^{-1}$ reported for PCL. ESI-MS spectra of poly(D,L-LA) showed some minor signals in addition to the main peaks (Fig. S15, ESI†) while that of poly(L-LA) showed mainly one signal corresponding to the mass of the lactide repeat unit (72 Da) (Fig. 8). The minor signals in the mass spectrum of poly(D,L-LA) are believed to originate from the transesterification process (back-biting) occurring in the system.[53–55]

The ring-opening polymerization of cyclic esters by metal-based catalysts is likely to proceed *via* either the coordination-insertion mechanism (CIM) or the activated-monomer mechanism (AMM).[56] In the CIM route, the polymer end chain bears the nucleophile on one end and the metal center on the other end. However, hydrolysis of one end of the polymer chain to form an –OH end group could be promoted by chain transfer agents such as water or alcohols.[57] To establish the nature of the initiating and chain-end groups in our system, $^1H$ NMR and ESI-MS spectra of poly(L-LA) obtained were analyzed. $^1H$ NMR spectra of all the polymers revealed the absence of acetate methyl signals at about 2.00 ppm (Fig. 8). Similarly, no signals associated with the ligand moiety in the complexes were observed. However, the ESI-MS spectra of poly(L-LA) showed signals indicating the presence of Zn–OH end groups, associated with the hydrolysis and ligand dissociation of the zinc complex (Fig. 9). These results are in agreement with those reported by Pilone and co-workers[58] in

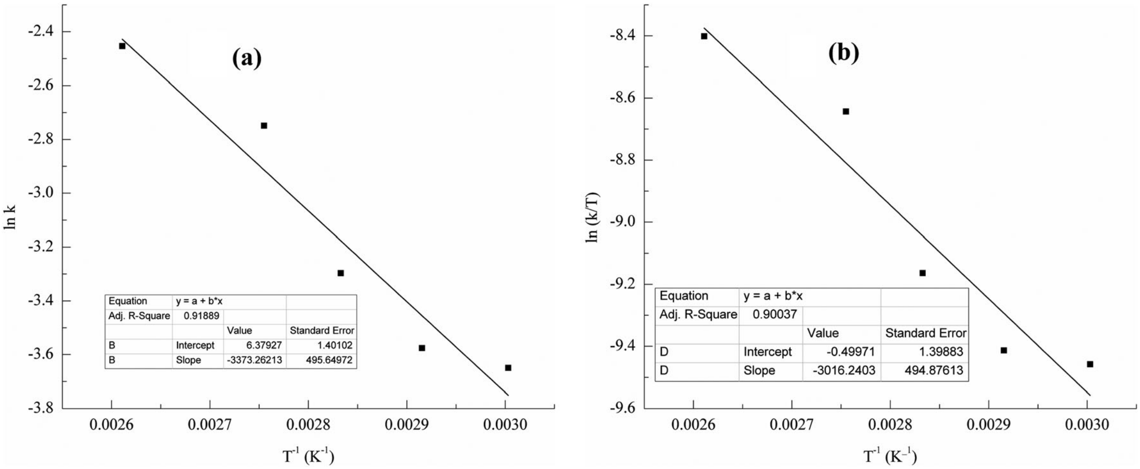

Fig. 7 (a) Arrhenius plot of ln *k* *vs.* $T^{-1}$ for the bulk polymerization of ε-CL initiated by **3**, M/I = 200. (b) Eyring plot of temperature dependence of the rate constant.

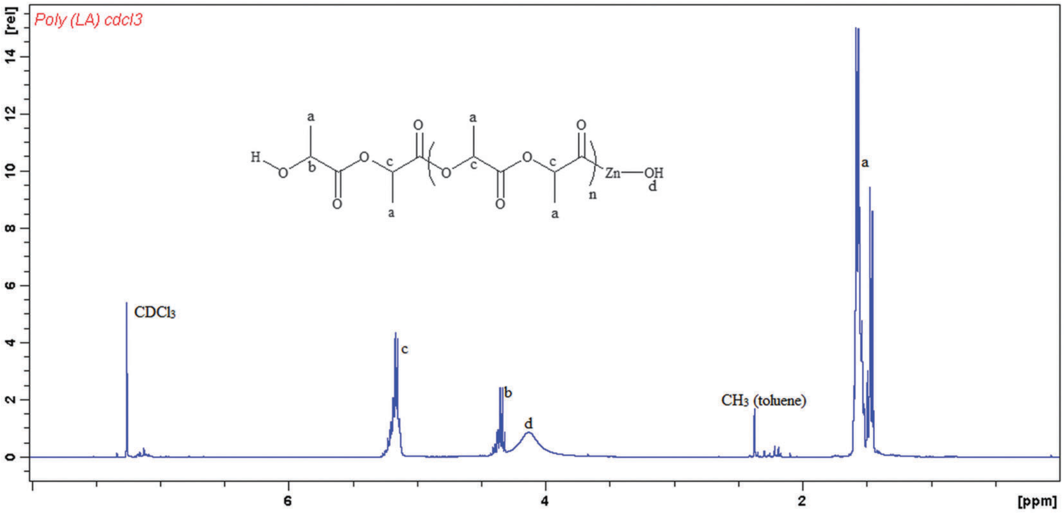

Fig. 8 $^1$H NMR spectrum of poly(L-LA) produced by complex **1**.

which water molecules hydrolyzed the polymer end chains. From these data, the polymerization reactions in our system can thus be said to proceed through the coordination insertion mechanism followed by hydrolysis of the acetate end groups.

A linear relationship of the plot of the molecular weight *versus* monomer conversion (Fig. 10) established the living polymerization behavior of these catalysts.[59,60] The observed increase in polymer weight with the increase in [CL]/[catalyst] ratio (low catalyst concentration) further supported this living polymerization nature (Table 3) and is consistent with a small number of active sites at lower concentration of the catalyst. Generally, the polymers obtained in this study exhibited narrow to moderate molecular weight distributions, 1.12–2.47 and 1.79–2.25 for PCLs and PLAs, respectively, indicating some degree of control of the ROP and minimal esterification and epimerization reactions.

The catalyst structure was also found to influence the molecular weights of the polymers obtained. Contrary to expectations,[36] increasing the steric bulk of the ligands resulted in decreased PCL molecular weights. For example, the molecular weight of 22 550 g mol$^{-1}$ was obtained using complex **1** bearing the less sterically demanding methyl substituents on the phenyl ring compared to the molecular weight of 9689 g mol$^{-1}$ observed for complex **2**, containing the bulkier isopropyl groups (Table 1, entries 1 and 2).[61,62]

We also noted the dependence of PCL molecular weight and molecular weight distributions on the identity of the solvent used in the ROP of ε-CL. Interestingly, PCL obtained in methanol solvent exhibited a narrow PDI of 1.12 compared to a PDI of 2.02 recorded in toluene solvent.

### Stereochemistry of polylactides

Poly(LA) tacticity was studied by inspecting the methine regions and tetrad sequences in the homonuclear decoupled $^1$H NMR and $^{13}$C NMR spectra of the polymers.[63] Fig. S16–S19 (ESI†) show the methine resonances of the homonuclear decoupled $^1$H and $^{13}$C NMR spectra of poly(L-LA) and poly(D,L-LA). The peaks were assigned to the appropriate tetrads in accordance with literature reports.[57] The *iii* tetrad is the predominant peak in the spectrum, thereby

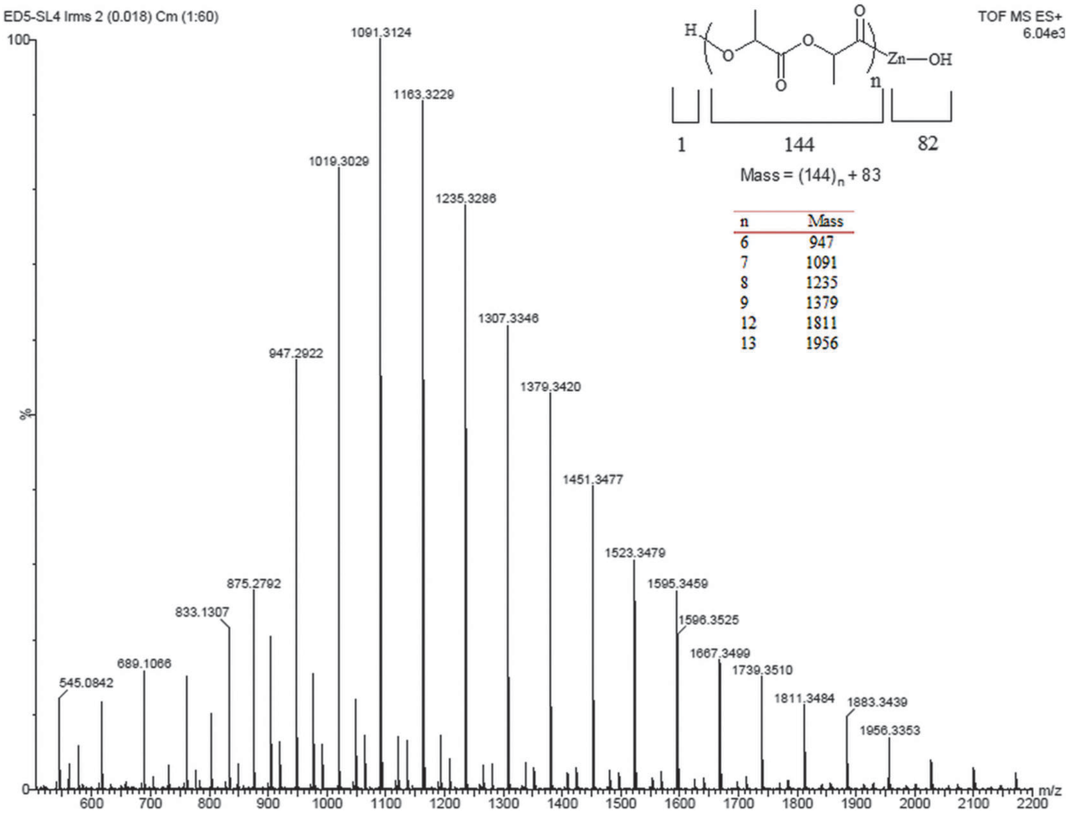

Fig. 9 ES-MS of the crude PLA (from L-LA) from catalyst **3**, $[CL]_0/[\mathbf{3}]$ = 200, 9 h, showing the distribution of signal corresponding to the mass of the lactide repeat unit.

yielding moderate isotactic poly(L-LA).[64] However, minor signals in the decoupled $^1$H NMR spectra could be attributed to the epimerization of the chiral centers, thus randomizing their absolute configuration and therefore resulting in the loss of control of polymer stereo-regularity.[57] We attempted to use homonuclear decoupled $^1$H NMR to quantify the number of defects in the poly(L-LA) chain. In the homonuclear decoupled $^1$H NMR spectra of the methine region of poly(L-LA) (Fig. S16, ESI†), the poly(L-LA) or the defect content was estimated from the total *iii* cored tetrad intensities by assuming a certain defect fraction and then continually corrected for changes in the defect fraction calculated from *iis* and *sis*/*sii* intensities.[65] Based on the composition analysis, we estimated the presence of 97.02% of poly(L-LA) and 2.98% of defects resulting from epimerization reactions. As reported in the literature,[65,66] a polymer sequence showing a characteristic resonance at $\delta$ = 5.21 ppm in a decoupled $^1$H NMR spectrum contains a single defect, whereas the stereoregular sequence shows a resonance at $\delta$ = 5.17 ppm. In addition, double stereo-defects show two characteristic resonances at $\delta$ = 5.22 and $\delta$ = 5.23 ppm, respectively. Considering the $^1$H homonuclear decoupled NMR of the methine region of poly(L-LA) formed with complexes **1** and **3**, respectively (Fig. S16, ESI†), it is therefore conceivable to state that the poly(L-LA) chain has double stereodefects arising from epimerization reactions. The core tetrad stereo-sequences in poly(D,L-LA) as given in Fig. S18 and S19 (ESI†) are well resolved and peak assignments are consistent with the literature[64,66] and the production of predominantly moderate heterotactic poly(D,L-LA) with Pr of up to 0.65.

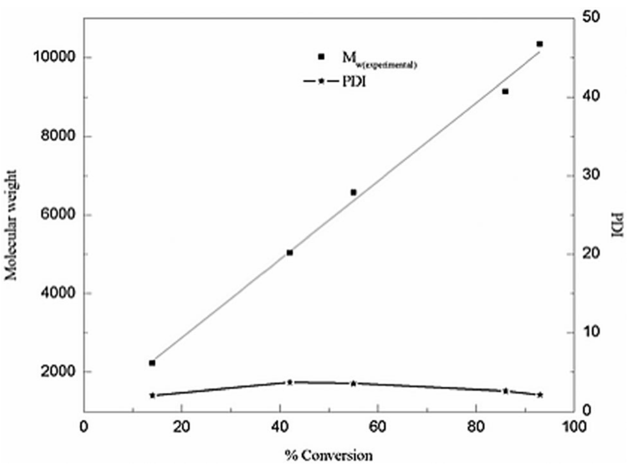

Fig. 10 Plot of experimental molecular weight against % conversion, showing the living polymerization nature of complex **3** in the bulk ROP of ε-CL at 110 °C, $[CL]_0/[I]$ = 200.

## Conclusions

This work demonstrates the coordination chemistry and the application of Zn(II) and Cu(II) formamidine complexes in the ring-opening polymerization of ε-caprolactone and lactides.

We have shown that the substituents on the phenyl ring of the ligand backbone significantly affect the coordination chemistry of the complexes to afford dinuclear and trinuclear complexes. Complexes **1–4** formed active and stable catalysts in the ring-opening polymerization of ε-caprolactone and D,L-lactide and L-lactide to produce polymers with moderate weights and molecular weight distributions. The catalytic activities of the complexes were largely controlled by the ligand architecture and metal atoms. The kinetics of the ROP reactions was *pseudo*-first order with respect to both ε-caprolactone and lactide monomers. Both the temperature and solvent significantly influenced the ring-opening polymerization of ε-caprolactone and an overall activation energy of 28.5 kJ mol$^{-1}$ was obtained. The catalysts display a reasonable degree of control of polymer stereoregularity producing predominantly heterotactic poly(D,L-lactide).

## Conflict of interest

The authors declare no competing financial interest.

## Acknowledgements

The authors would like to thank the College of Agriculture, Science and Engineering, University of KwaZulu-Natal, and National Research Foundation (NRF), South Africa for financial support.

## References

1 S. Kasirajan and M. Ngouajio, *Agron. Sustainable Dev.*, 2012, **32**, 501–529.
2 W. Amass, A. Amass and B. Tighe, *Polym. Int.*, 1998, **47**, 89–144.
3 K. E. Uhrich, S. M. Cannizzaro, R. S. Langer and K. M. Shakesheff, *Chem. Rev.*, 1999, **99**, 3181–3198.
4 Y. Ikada and H. Tsuji, *Macromol. Rapid Commun.*, 2000, **21**, 117–132.
5 A.-C. Albertsson and I. K. Varma, *Biomacromolecules*, 2003, **4**, 1466–1486.
6 N. E. Kamber, W. Jeong, R. M. Waymouth, R. C. Pratt, B. G. G. Lohmeijer and J. L. Hedrick, *Chem. Rev.*, 2007, **107**, 5813–5840.
7 A. P. Gupta and V. Kumar, *Eur. Polym. J.*, 2007, **43**, 4053–4074.
8 C. A. Wheaton, P. G. Hayes and B. J. Ireland, *Dalton Trans.*, 2009, 4832–4846.
9 H.-Y. Chen, B.-H. Huang and C.-C. Lin, *Macromolecules*, 2005, **38**, 5400–5405.
10 M. Cheng, A. B. Attygalle, E. B. Lobkovsky and G. W. Coates, *J. Am. Chem. Soc.*, 1999, **121**, 11583–11584.
11 F. Drouin, P. O. Oguadinma, T. J. J. Whitehorne, R. E. Prud'homme and F. Schaper, *Organometallics*, 2010, **29**, 2139–2147.
12 S. Collins, *Coord. Chem. Rev.*, 2011, **255**, 118–138.
13 L. F. Sanchez-Barba, C. Alonso-Moreno, A. Garces, M. Fajardo, J. Fernandez-Baeza, A. Otero, A. Lara-Sanchez, A. M. Rodriguez and I. Lopez-Solera, *Dalton Trans.*, 2009, 8054–8062.
14 F. T. Edelmann, in *Adv. Organomet. Chem.*, ed. F. H. Anthony and J. F. Mark, Academic Press, 2008, vol. 57, pp. 183–352.
15 S. Schmidt, S. Schulz, D. Bläser, R. Boese and M. Bolte, *Organometallics*, 2010, **29**, 6097–6103.
16 C. M. Thomas, *Chem. Soc. Rev.*, 2010, **39**, 165–173.
17 S. O. Ojwach, T. T. Okemwa, N. W. Attandoh and B. Omondi, *Dalton Trans.*, 2013, **42**, 10735–10745.
18 J. Wang, Y. Yao, Y. Zhang and Q. Shen, *Inorg. Chem.*, 2009, **48**, 744–751.
19 J. Wang, T. Cai, Y. Yao, Y. Zhang and Q. Shen, *Dalton Trans.*, 2007, 5275–5281.
20 Y. Luo, P. Xu, Y. Lei, Y. Zhang and Y. Wang, *Inorg. Chim. Acta*, 2010, **363**, 3597–3601.
21 K. Phomphrai, C. Pongchan-o, W. Thumrongpatanaraks, P. Sangtrirutnugul, P. Kongsaeree and M. Pohmakotr, *Dalton Trans.*, 2011, **40**, 2157–2159.
22 Bruker, *APEXII Bruker AXS Inc.*, 2009, Madison, Wisconsin, USA.
23 Bruker, *SAINT Bruker AXS Inc.*, 2009, Madison, Wisconsin, USA.
24 Bruker, *Bruker SADABS Bruker AXS Inc.*, 2009, Madison, Wisconsin, USA.
25 G. Sheldrick, *Acta Crystallogr., Sect. A: Found. Crystallogr.*, 2008, **64**, 112–122.
26 O. V. Dolomanov, L. J. Bourhis, R. J. Gildea, J. A. K. Howard and H. Puschmann, *J. Appl. Crystallogr.*, 2009, **42**, 339–341.
27 T. Elkin, N. V. Kulkarni, B. Tumanskii, M. Botoshansky, L. J. W. Shimon and M. S. Eisen, *Organometallics*, 2013, **32**, 6337–6352.
28 E. C. Taylor and W. A. Ehrhart, *J. Org. Chem.*, 1963, **28**, 1108–1112.
29 J. Zhang, K. Higashi, K. Ueda, K. Kadota, Y. Tozuka, W. Limwikrant, K. Yamamoto and K. Moribe, *Int. J. Pharm.*, 2014, **465**, 255–261.
30 U. Kumar, J. Thomas and N. Thirupathi, *Inorg. Chem.*, 2009, **49**, 62–72.
31 M. Devereux, D. O'Shea, M. O'Connor, H. Grehan, G. Connor, M. McCann, G. Rosair, F. Lyng, A. Kellett, M. Walsh, D. Egan and B. Thati, *Polyhedron*, 2007, **26**, 4073–4084.
32 G. Parkin, *Chem. Rev.*, 2004, **104**, 699–768.
33 J.-C. Wu, B.-H. Huang, M.-L. Hsueh, S.-L. Lai and C.-C. Lin, *Polymer*, 2005, **46**, 9784–9792.
34 N. W. Attandoh, S. O. Ojwach and O. Q. Munro, *Eur. J. Inorg. Chem.*, 2014, 3053–3064.
35 J. Börner, U. Flörke, A. Döring, D. Kuckling, M. Jones and S. Herres-Pawlis, *Sustainability*, 2009, **1**, 1226–1239.
36 L. Wang, W. Qin and W. Liu, *Inorg. Chem. Commun.*, 2010, **13**, 1122–1125.
37 Y.-P. Huo, S.-Z. Zhu and S. Hu, *Tetrahedron*, 2010, **66**, 8635–8640.
38 G. Zhang, S. Wang, Q. Gan, Y. Zhang, G. Yang, J. Shi Ma and H. Xu, *Eur. J. Inorg. Chem.*, 2005, 4186–4192.
39 R.-H. Hui, P. Zhou and Z.-L. You, *Indian J. Chem., Sect. A: Inorg., Bio-inorg., Phys., Theor. Anal. Chem.*, 2009, **48A**, 663–667.
40 G. Yuan, Y. Huo, X. Nie, H. Jiang, B. Liu, X. Fang and F. Zhao, *Dalton Trans.*, 2013, **42**, 2921–2929.
41 P. D. Knight, A. J. P. White and C. K. Williams, *Inorg. Chem.*, 2008, **47**, 11711–11719.
42 P. Maiti, A. Khan, T. Chattopadhyay, S. Das, K. Manna, D. Bose, S. Dey, E. Zangrando and D. Das, *J. Coord. Chem.*, 2011, **64**, 3817–3831.

43 J. C. Stephens, M. A. Khan and R. P. Houser, *Inorg. Chem.*, 2001, **40**, 5064–5065.

44 G. F. Kokoszka, M. Linzer and G. Gordon, *Inorg. Chem.*, 1968, **7**, 1730–1735.

45 B. J. O'Keefe, L. E. Breyfogle, M. A. Hillmyer and W. B. Tolman, *J. Am. Chem. Soc.*, 2002, **124**, 4384–4393.

46 L. M. Hodgson, R. H. Platel, A. J. P. White and C. K. Williams, *Macromolecules*, 2008, **41**, 8603–8607.

47 D. Appavoo, B. Omondi, I. A. Guzei, J. L. van Wyk, O. Zinyemba and J. Darkwa, *Polyhedron*, 2014, **69**, 55–60.

48 A. Duda and A. Kowalski, *Handbook of Ring-Opening Polymerization*, Wiley-VCH Verlag GmbH & Co. KGaA, 2009, pp. 1–51.

49 Y. Mei, A. Kumar and R. Gross, *Macromolecules*, 2003, **36**, 5530–5536.

50 L. Zhang, Y. Niu, Y. Wang, P. Wang and L. Shen, *J. Mol. Catal. A: Chem.*, 2008, **287**, 1–4.

51 D. J. Darensbourg, P. Ganguly and D. Billodeaux, *Macromolecules*, 2005, **38**, 5406–5410.

52 H. Sun, J. S. Ritch and P. G. Hayes, *Dalton Trans.*, 2012, **41**, 3701–3713.

53 P. Dubois, C. Jacobs, R. Jerome and P. Teyssie, *Macromolecules*, 1991, **24**, 2266–2270.

54 K. Kim, J. Lee, T. Chang and H. Kim, *J. Am. Soc. Mass Spectrom.*, 2014, **25**, 1771–1779.

55 D. C. Aluthge, J. M. Ahn and P. Mehrkhodavandi, *Chem. Sci.*, 2015, **6**, 5284–5292.

56 J. Wu, T.-L. Yu, C.-T. Chen and C.-C. Lin, *Coord. Chem. Rev.*, 2006, **250**, 602–626.

57 T. M. Ovitt and G. W. Coates, *J. Polym. Sci., Part A: Polym. Chem.*, 2000, **38**, 4686–4692.

58 A. Pilone, M. Lamberti, M. Mazzeo, S. Milione and C. Pellecchia, *Dalton Trans.*, 2013, **42**, 13036–13047.

59 W.-L. Kong and Z.-X. Wang, *Dalton Trans.*, 2014, **43**, 9126–9135.

60 H. V. Babu and K. Muralidharan, *RSC Adv.*, 2014, **4**, 6094–6102.

61 S. A. Svejda, L. K. Johnson and M. Brookhart, *J. Am. Chem. Soc.*, 1999, **121**, 10634–10635.

62 L. Deng, T. K. Woo, L. Cavallo, P. M. Margl and T. Ziegler, *J. Am. Chem. Soc.*, 1997, **119**, 6177–6186.

63 M. T. Zell, B. E. Padden, A. J. Paterick, K. A. M. Thakur, R. T. Kean, M. A. Hillmyer and E. J. Munson, *Macromolecules*, 2002, **35**, 7700–7707.

64 Y. Yang, H. Wang and H. Ma, *Inorg. Chem.*, 2015, **54**, 5839–5854.

65 K. A. M. Thakur, R. T. Kean, E. S. Hall, M. A. Doscotch and E. J. Munson, *Anal. Chem.*, 1997, **69**, 4303–4309.

66 K. A. M. Thakur, R. T. Kean, E. S. Hall, J. J. Kolstad, T. A. Lindgren, M. A. Doscotch, J. I. Siepmann and E. J. Munson, *Macromolecules*, 1997, **30**, 2422–2428.